

# UGG: Unified Generative Grasping

Jiaxin Lu<sup>1</sup> Hao Kang<sup>2</sup> Haoxiang Li<sup>2</sup> Bo Liu<sup>2</sup> Yiding Yang<sup>2</sup>  
 Qixing Huang<sup>1</sup> Gang Hua<sup>2</sup>

<sup>1</sup> The University of Texas at Austin <sup>2</sup> Wormpex AI Research

## Abstract

Dexterous grasping aims to produce diverse grasping postures with a high grasping success rate. Regression-based methods that directly predict grasping parameters given the object may achieve a high success rate but often lack diversity. Generation-based methods that generate grasping postures conditioned on the object can often produce diverse grasping, but they are insufficient for high grasping success due to lack of discriminative information. To mitigate, we introduce a unified diffusion-based dexterous grasp generation model, dubbed the name UGG, which operates within the object point cloud and hand parameter spaces. Our all-transformer architecture unifies the information from the object, the hand, and the contacts, introducing a novel representation of contact points for improved contact modeling. The flexibility and quality of our model enable the integration of a lightweight discriminator, benefiting from simulated discriminative data, which pushes for a high success rate while preserving high diversity. Beyond grasp generation, our model can also generate objects based on hand information, offering valuable insights into object design and studying how the generative model perceives objects. Our model achieves state-of-the-art dexterous grasping on the large-scale DexGraspNet dataset while facilitating human-centric object design, marking a significant advancement in dexterous grasping research. Our project page is <https://jiaxin-lu.github.io/ugg/>.

## 1. Introduction

The significance of robotic grasping is underscored by its ability to foster a human-like interaction between robotic systems and the environment, playing a fundamental role in supporting robots across a diverse range of tasks—from straightforward pick-and-place operations [4] to intricate assembly processes [12]. The increased interest in dexterous grasping comes from its ability to anthropomorphically grasp objects of diverse shapes and sizes [1, 65, 77, 83]. This capability not only improves the execution of downstream

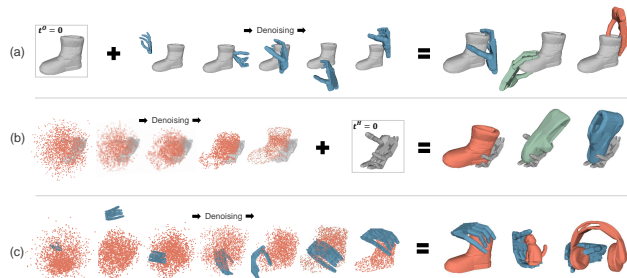


Figure 1. Overview of three tasks performed by the proposed UGG model: (a) Generating grasps with a fixed object involves denoising hand parameters and transformations for diverse successful postures. (b) Generating objects with a fixed hand posture denoises shape latents for varied object fits. (c) Jointly generating hand posture and object involves simultaneous denoising of both latents, yielding diverse grasps with objects.

tasks, but also broadens the scope of robotic applications, including manufacturing, agriculture, healthcare, and extended reality [13, 19, 24, 31, 79].

In order to deal with the dynamically changing environment for planning [70, 77], dexterous grasping aims to produce diverse grasping postures with a high grasping success rate. Before the emergence of large datasets, the field of robotic grasping relied primarily on analytical-based methods, including force closure optimization [11], and simulation-based techniques, such as differentiable contact simulation [65]. With large-scale datasets such as DexGraspNet [71], data-driven approaches have become the focus, generally falling into two main categories, regression-based methods and generation-based methods.

Regression-based methods, as exemplified by DDG [33], directly predict the grasp parameters given the object as input, which is prone to either mode collapse, which hurts diversity, or mode averaging, which degrades regression accuracy and hence success rate. On the contrary, generation-based methods, such as GraspTTA [21], excel at producing a wider variety of grasping strategies. However, because they lack discriminative information on whether grasping could be a success, their success rate may not be sufficient.

To mitigate these insufficiencies, we propose a diffusion-based grasping generation model to guarantee grasp diver-

sity, which is complemented by a simple physics discriminator to push for a high success rate. Our model operates in a latent space of 3D object point clouds and hand-joint parameters, explicitly focusing on diffusing hand positioning and *Contact Anchor*. The anchors are designed to transform the conventional intermediate format of the contact map [15, 21, 34] into a representation that not only aligns with the shape but can also be seamlessly integrated into the generation process. Furthermore, we employ an all-transformer architecture to unify the three elements - object, hand, and contact - into a single unified diffusion model.

Beyond grasp generation, our unified diffusion model exhibits expanded capabilities, generating hand and contact anchors from provided objects and reciprocally creating objects and their associated contact information based on given hand poses, as illustrated in Fig. 1. The generated shapes provide insightful perspectives on how the model perceives objects, thereby enhancing the interpretability of the generation outcomes and facilitating a more effective design of object representations. In addition, qualitative experiments indicate that this model can produce valid solutions for the human-centric design of objects.

In summary, our main contributions are as follows.

- We introduce a unified diffusion model UGG for investigating hand-object interaction tasks through a perspective of generation. Our model seamlessly brings grasping, object generation, and affordance analysis into a cohesive framework.
- We propose a new contact anchors representation instead of using the conventional contact map as navigational cues for affordance information. This representation aligns harmoniously with the point cloud representation, enabling effective participation in the multi-modal generative tasks.
- Leveraging the diversity and validation rate of our model, we introduce a physics discriminator to assess the success of hand-object grasping, achieving state-of-the-art performance in the grasp generation task.
- In particular, UGG exhibits the unique ability to generate objects based on given hand parameters. This not only advances research on object representations in hand-object interaction tasks but also paves the way for human-centric object design studies.

## 2. Related Work

**Dexterous Grasping.** Analytical and simulation-based multi-finger grasping methods [10, 11, 27, 35, 45, 49, 51, 54, 65] were extensively investigated prior to the advent of large-scale datasets [66, 71], which exhibit limited generalizability or require heavy computing. Data-driven approaches [47], whether directly regressing grasp based on the object [32, 33, 53] or using generative models for grasp

synthesis [21, 38, 39, 73], frequently confront the dilemma of balancing diversity and quality. Meanwhile, contact information is frequently used indirectly as a bridge [5, 15, 22, 28, 29, 34, 44, 58, 68, 84] to improve grasp quality.

**Diffusion Models.** Diffusion models represent a significant advancement in image generation [17, 23, 52, 55, 56, 60, 62, 64, 80]. Expanding into the 3D domain, diffusion models have shown great success in generating point clouds [40, 78, 81], meshes [16, 36], signed distance functions [8, 9], and neural fields [46, 59], facilitating high-quality and controllable 3D synthesis [30, 41, 74]. We adopt the VAEs [26] of LION [78] to produce the object representation, which excels in the precise reconstruction of point clouds. The hierarchical latent representation of these VAEs facilitates the subsequent diffusion-based generation of both hand posture and object.

Diffusion models effectively handle spatial connection-based generative challenges, as evidenced by molecular design [75], layout generation [6, 72], gripper pose generation [67] and scene synthesis and planning [20]. Methods in [20, 67] exhibit similarities in diffusion grasping, but our proposed model can simultaneously generate both object and hand. While gripper [67] has fewer parameters, it is not geared for dexterous grasping. The SceneDiffuser [20], though is able to handle dexterous grasping, lacks modeling grasp-specific context, *e.g.*, contact, affecting posture quality. In addition, it conditions posture by object with cross-attention [69], which does not sufficiently consider the alignment of manifold priors [3, 76], is insufficient in dealing with colliding and floating poses.

## 3. Problem and Our Approach

### 3.1. Problem Statement

In a broad sense, dexterous grasping is a multistage process that encompasses various aspects such as perception, motion planning, and execution. In a narrow sense, it refers to the process of producing hand postures that can successfully grasp an object. Following the literature, we address it from a narrow sense. More specifically, we assume that the representation of the given object  $\mathbf{o}$  is a point cloud, *e.g.*,  $\mathbf{o} \in \mathbb{R}^N \times 3$ . Let  $\mathbf{h} = (\boldsymbol{\theta}, \mathbf{R}, \mathbf{t})$  represent a posture of the hand, where  $\mathbf{R} \in \text{SO}(3)$  and  $\mathbf{t} \in \mathbb{R}^3$  denote root rotation and translation,  $\boldsymbol{\theta} \in \mathbb{R}^k$  represent the joint angles of the hand model, with  $k$  denoting the degree of freedom (*e.g.*,  $k = 22$  for the adopted ShadowHand [57] model).

The objective of dexterous grasping is to produce a diverse set  $\mathbb{H} = \{\mathbf{h}_i\}_{i=1}^m$  of articulated hand postures that can grasp the target object  $\mathbf{o}$  with a high success rate. An ideal method would produce a highly diverse set of grasping with a high success rate. The definition of what a successful grasp is and the quantification of the diversity of the produced grasping  $\mathbb{H}$  could depend on the application. We

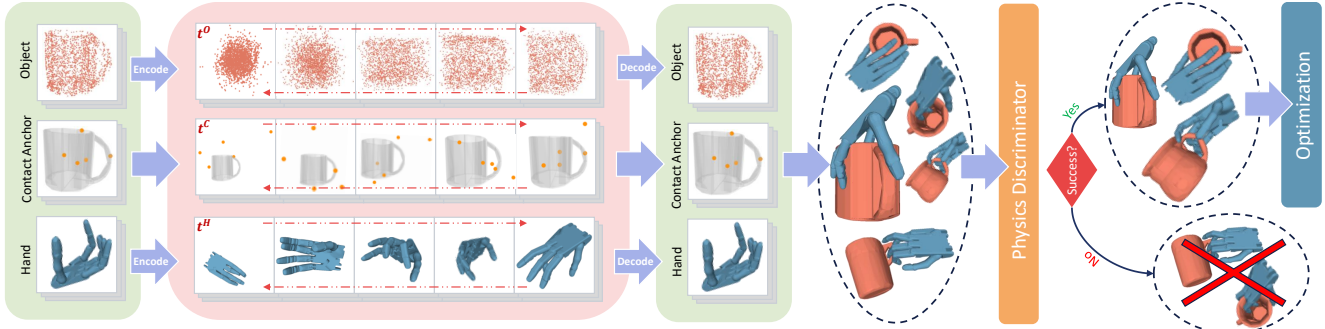


Figure 2. Overview of the proposed method UGG: Our approach involves encoding and embedding the object, contact anchors, and hand to facilitate the learning of a unified diffusion model. During inference, random seeds are sampled and subjected to a denoising process to generate samples. To discern potentially successful grasps, a physics discriminator is introduced. Subsequently, an optimization stage is undertaken for all selected grasps, utilizing the generated contact anchor and input point cloud.

follow the definition and quantification presented by Wang et al. [71]. In particular, a grasp is considered a success “if it can withstand at least one of the six gravity directions and has a maximum penetration of less than 5mm [71]”. The diversity of the produced grasps is measured by the entropy of the joint angles of the generated grasp postures.

### 3.2. Overview of Our Approach

As shown in Fig. 2, our formulation approaching the dexterous grasping problem is composed of two main parts. The first part is a unified diffusion model which jointly models the generation of grasping hands, objects, and their contact information, which is capable of generating a diverse set of candidate grasping postures given an object of interest. The second part is a lightweight discriminative classifier trained from simulation data that entails discriminative information on whether a grasp is a success.

**Unified Grasping Generator.** In the natural shape space, dexterous grasping involves three elements, *e.g.*, the *articulated grasping hand*, the *object*, and the *contact* between the two. We regard the problem of dexterous grasping as the interaction among three data manifolds, *i.e.*, the manifold of the articulated grasping hands, and that of the objects, aligned by the manifold of the contact.

Therefore, the question arises as to how to effectively model the interactions among the three manifolds. There are several factors to consider to establish an effective model. The first is how to represent the three manifolds in latent space that effectively model their structures, *e.g.* latent embeddings. The next question is how to model the interactions of the three manifolds to effectively leverage the interaction irregularity in the training data.

As discussed in Sec. 3.1, objects are represented as point clouds, and hands are tuples that include joints and rigid 3D translations. Following LION [78], objects and hands are encoded as shape-latent codes by variational auto-encoders (VAE) [26], details included in Sec. 4.1.

For contact modeling, most previous methods have used the contact map, contact parts, and direction [15, 21, 22, 34].

These representations are typically continuous, posing a challenge in their applicability to the unordered set nature of point clouds during the generative process. The diffusion process does not preserve the mapping between the contact and point cloud. We found a very simple but very effective new representation, *Contact Anchor*, which characterizes the contact information as a set of  $N_c$  contact anchors, *e.g.*,  $c \in \mathbb{R}^{N_c \times 3}$ . Please refer to Sec. 4.2 for details.

To effectively model the interaction among the three manifolds, we cast them into a unified diffusion model by fitting one transformer to model all distributions. Inspired by UniDiffuser [3], we use its transformer-based backbone, known as U-ViT [2], to serve as the core of our joint noise prediction network. Depicted in Fig. 2, the denoising process is trained on asynchronous scheduling of different manifolds, formulating all conditional, marginal, and joint distributions. The UniDiffuser samples combinations of hands and objects not restricted to training data, facilitating a generative model with high generalization capability.

Specifically, the generation behavior can be manipulated by carefully adjusting the sampling scheduler. Fig. 1 shows different generation modes: hand generation by fixing step 0 to the object scheduler (a), object generation by fixing step 0 to the hand scheduler (b), and combined generation without fixing any scheduler (c).

**Physics Discriminator.** The unified diffusion model is capable of producing a diverse set of grasping postures. However, we can not neglect the hallucination phenomenon, which implies that a significant portion of the generated candidate grasping may not produce a successful grasp.

Given sufficient discriminative guidance, a classifier could be learned to predict whether a candidate’s posture would be able to successfully grasp the target object or not. However, discriminative guidance, *e.g.*, the label of whether a grasp would be successful, is not readily available. To obtain such discriminative labels for training, we resort to the physics simulator, Isaac Gym [43], to judge whether a rendered candidate would compose a successful grasping. This discriminator takes advantage of the diversity of the re-

sults generated and significantly improves the success rate of grasping, shown in Sec. 6.

## 4. Formulation

The proposed framework comprises three components. First, the embeddings of objects and hands (Sec. 4.1), bridged by the novel contact modeling (Sec. 4.2), formulate a unified representation in latent space. Then, a unified diffusion model (Sec. 4.3) is trained to generate effective and diversified grasping. Finally, a discriminator (Sec. 4.4) is meticulously formulated to ensure a high success rate in hand generation without compromising diversity.

### 4.1. Unified Shape Encoding

**Objects** are depicted as point clouds in natural-shape space and hybrid embeddings in latent space. As shown in [78], a hierarchical VAE is capable of capturing global shapes across categories with various scales, while maintaining details for precise reconstruction. Moreover, its latent representation is suitable for diffusion models, facilitating the generation of diverse shapes.

Specifically, given a point cloud  $\mathbf{o} \in \mathbb{R}^{N \times 3}$ , a global embedding  $\mathbf{g}_o \in \mathbb{R}^{d_g}$  is obtained by a global encoder. A local encoder maps each point in the point cloud to a  $d_l$  dimensional local feature regulated by the global embedding, resulting in a local representation  $\mathbf{l}_o \in \mathbb{R}^{N \times (3+d_l)}$ . The hybrid embedding of an object  $\mathbf{x}_o = \mathbf{g}_o \oplus \mathbf{l}_o$  is a concatenation of global and local latent codes. Subsequently, a decoder is introduced to reconstruct the latent representation  $\mathbf{x}_o$  into its point cloud. The architecture of the encoders and decoders adheres closely to the Point-Voxel CNNs (PVCNNs) [37] framework, which was also utilized in LION [78].

**Hands** are parameterized as a tuple  $(\boldsymbol{\theta}, \mathbf{R}, \mathbf{t})$ , where  $\boldsymbol{\theta} \in \mathbb{R}^k$  are joint angles from ShadowHand [57],  $\mathbf{R} \in \text{SO}(3)$  and  $\mathbf{t} \in \mathbb{R}^3$  denote 3D rotation and translation. In order to encourage a semantic embedding that facilitates easy reconstruction, a latent code representing the shape of the hand is encoded from  $\boldsymbol{\theta}$  to ensure its independence from rigid transformations. Similar to the global embedding of an object, VAE is used with the decoder parameterized as a factorial Gaussian distribution corresponding to an  $L_2$  reconstruction loss, resulting in a latent shape code  $\mathbf{g}_h$ . Adding 3D rotation and translation, the final hand representation is  $\mathbf{x}_h = \mathbf{g}_h \oplus \mathbf{r} \oplus \mathbf{t}$ , where  $\mathbf{r}$  is the flattened rotation matrix  $\mathbf{R}$ , and  $\oplus$  is the concatenation of features.

### 4.2. Unified Contact Modeling

Object and hand encoders are individually trained to facilitate their own shape reconstruction, without aligning together for good grasping. As shown in Fig. 3, a subtle change in the object can cause grasping failure. The corresponding change in latent representation may not be significant enough to capture critical detail. This underscores



Figure 3. Subtle object changes can lead to grasping failure, as the corresponding adjustment in latent representation may not capture critical details adequately.

the need to incorporate contact information into the unified representation.

Previous approaches have taken two main routes to capture this information. Pre-processing methods [15, 22, 34] generate contact information directly before employing optimization algorithms to fit a hand model. The post-processing approach, e.g., GraspTTA [21], involves a two-stage training process to first compute a possible contact map based on an initial hand estimate, and then refine the pose on it. Unfortunately, neither of the existing contact modelings successfully accomplishes the joint generation of both hand parameters and a contact model.

We propose *Contact Anchor* as a novel modality to convey contact information. It is a set of points located on the meshes of both the object and the hand. In practice, given the distance of a point  $\mathbf{c}$  to a mesh  $\mathbf{S}$  as:

$$d(\mathbf{c}, \mathbf{S}) = \min_i \|\mathbf{c} - \mathbf{s}_i\|_2, \quad \forall \mathbf{s}_i \in \mathbf{S}, \quad (1)$$

*Contact Anchor*,  $\mathbf{c} \in \mathbb{R}^{N_c \times 3}$ , is composed by randomly selecting  $N_c$  points from the object point cloud  $\mathbf{p}_o$ , such that the distance to the hand mesh  $\mathbf{S}_h$  is below a threshold  $\eta$ :

$$\mathbf{c} = [\mathbf{c}_1, \dots, \mathbf{c}_{N_c}], \quad \mathbf{c}_i \in_R \{d(\mathbf{c}, \mathbf{S}_h) < \eta | \mathbf{c} \in \mathbf{p}_o\}, \quad (2)$$

where  $\in_R$  denotes uniformly random sampling of elements from a set.

This design avoids the extensive calculation of mesh intersection, while explicitly revealing grasping patterns. Represented as a set of points, *Contact Anchor* facilitates seamless integration and easy reconstruction through the proposed unified diffusion framework.

### 4.3. Unified Generation

UniDiffuser [3] explored a unified perspective on the diffusion model by fitting one transformer to model all distributions. Given our objective of aligning three distributions, specifically object, hand, and contact information, this approach seamlessly aligns with the intuition behind UniDiffuser. Therefore, we leverage its transformer-based backbone, known as U-ViT [2], to serve as the core for our joint noise prediction network.

In our effort to align all distributions using U-ViT, a crucial step in employing transformer-based methods is to tokenize each representation, with each token embedded in

$\mathbb{R}^d$ . The global embedding  $g_o$  of the object point cloud is mapped naturally into a single token. Due to its high dimension, the local embedding, however, is downsampled to  $N_l$  tokens by farthest point sampling and k-nearest-neighbor grouping [50]. For hand  $(g_h, r, t)$ , each component is embedded independently into a token, and for contact anchors  $c$ , each point is represented by one token. In general, an object representation  $o$  with  $N_l + 1$  tokens, a hand code  $h$  with 3 tokens, and a contact map  $c$  with  $N_c$  tokens are combined as reconstruction data from the unified diffusion pipeline.

We hereby introduce a unified formulation that includes the conditional distributions  $q(o_0, h_0 | c_0)$ ,  $q(o_0, c_0 | h_0)$ ,  $q(c_0, o_0 | h_0)$ ,  $q(o_0 | h_0, c_0)$ ,  $q(h_0 | o_0, c_0)$ ,  $q(c_0 | o_0, h_0)$ , and the joint distribution  $q(o_0, h_0, c_0)$ . To achieve this, we introduce the concept of *asynchronized timesteps* for the data, denoted as  $t^o$ ,  $t^h$  and  $t^c$ . Expectations modeling takes on a general form expressed as  $\mathbb{E}[\epsilon^o, \epsilon^h, \epsilon^c | o_{t^o}, h_{t^h}, c_{t^c}]$ . Specifically, when  $t^o = 0$ ,  $\mathbb{E}[\epsilon^h, \epsilon^c | o_0, h_{t^h}, c_{t^c}]$  corresponds to the conditional distribution  $q(h_0, c_0 | o_0)$ , e.g., grasping generation, visualized in Fig. 1(a).

By denoting  $ohc = (o, h, c)$ ,  $t = (t^o, t^h, t^c)$ ,  $\epsilon = [\epsilon^o, \epsilon^h, \epsilon^c]$  and  $ohc_t = (o_{t^o}, h_{t^h}, c_{t^c})$ , within the unified perspective of diffusion models, our objective is formulated as

$$\mathbb{E}_{ohc_0, t, \epsilon} \|\epsilon_\xi(ohc_t, t) - \epsilon\|_2^2, \quad (3)$$

where  $\xi$  is the parameters of the noise prediction deep neural network. It is essential to note that this formulation provides a cohesive and integrated framework, allowing us to seamlessly model hand-object interactions from a generative perspective using a single model.

#### 4.4. Discriminator

The proposed unified model generates grasping configurations conditioned on given objects. While providing high diversity in potential postures, generative models contend with a diminished success rate, due to the absence of deterministic objectives during training.

Specifically, the evaluation process involves a physical simulator, Isaac Gym [43], to determine the grasping quality. The simulator is not differentiable and, therefore, cannot be implemented as an objective during training. To mitigate this gap between training and evaluation, a lightweight recognition model, termed a *Physics Discriminator*, is introduced as an efficient component for the purpose of identifying successful samples among the generated postures. This incorporation harnesses the high diversity and propels towards an enhanced success rate of grasping.

A notable challenge arises from the fact that existing datasets inherently contain only valid grasping, without any invalid samples during the discriminator’s training. Fortunately, with the generative nature of the proposed model, adversarial samples with substantial coverage can be obtained from a suboptimal model (e.g., an early-stage

model). The ground truths for training are acquired by the physical simulator, with successful grasping as  $y = [0, 1]^T$ , and unsuccessful as  $y = [1, 0]^T$ . Given an object point cloud  $o$  and a generated hand  $\hat{h}$ , physical discriminator  $D$  is trained with a cross-entropy loss:

$$\mathcal{L}_{\text{dis}}(o, \hat{h}, y) = - \sum_{i=0}^1 y_i \log \frac{\exp[D(o, \hat{h})_i]}{\sum_{j=0}^1 \exp[D(o, \hat{h})_j]}. \quad (4)$$

## 5. Learning and Inference

**Learning.** The training of the entire framework can be divided into three stages. In the first stage, VAEs are trained individually to obtain latent representations of objects and hands. Then, a unified diffusion is trained to minimize Eq. 3. Finally, the physical discriminator is optimized on the grasping results generated within the training set.

**Inference.** In the inference stage, given the target object (a.k.a., setting its diffusion branch to constant time step  $t^o$ ), we run the proposed unified diffusion model to obtain a diverse set of  $M$  candidate grasping hands. Then we feed the  $M$  candidate grasping hands to the discriminator, and the top  $N$  candidates with the highest classification scores are picked up as output. Furthermore, we adopt the *test-time adaptation* from [21] to ensure physically plausible results. More specifically, given *Contact Anchor*  $c = [c_1, \dots, c_{N_c}]$ , the contact loss is defined as  $\mathcal{L}_{\text{cont}} = \sum_{i=1}^{N_c} d(c_i, S_h)$ . The overall loss in test-time optimization is

$$\mathcal{L}_{\text{test}} = \omega_{\text{pen}} \mathcal{L}_{\text{pen}} + \omega_{\text{spen}} \mathcal{L}_{\text{spen}} + \omega_{\text{joint}} \mathcal{L}_{\text{joint}} + \omega_{\text{cont}} \mathcal{L}_{\text{cont}}, \quad (5)$$

where  $\mathcal{L}_{\text{pen}}$ ,  $\mathcal{L}_{\text{spen}}$ , and  $\mathcal{L}_{\text{joint}}$  are penetration, self-penetration and joint angle losses from [71] and [21]. We optimize the loss function through gradient descent using ADAM [25] for 100 steps.

## 6. Experiment and Evaluation

### 6.1. Experimental Setup

**Dataset.** We evaluate our method using the DexGrasp-Net [71], a challenging large-scale dexterous grasping benchmark. It encompasses 1.32 million dexterous grasps on 5355 objects, following the structure of Shadow-Hand [57]. Each object is associated with over 200 grasps, and the dataset is curated through an optimization algorithm. Rigorous validation is conducted in the Isaac Gym simulator [43] and on the penetration depth, ensuring the effectiveness and reliability of all grasps. The training set consists of 4229 objects, while the test set consists of 1126 objects among which 236 objects are considered objects from novel categories.

Given the complex nature of this dataset, we employ two subsets to generate results and conduct the ablation study. The first subset, referred to as “20 objects”, comprises a

training and testing set featuring 20 carefully selected objects in 12 categories, including two novel objects in the testing set. This subset plays a crucial role in our ablation study and serves as the basis for constructing the object generation model. The second subset, termed “10 bottles”, specifically includes 10 bottles for training the object and the joint generation model. This choice aligns with previous studies on point cloud generation [42, 78], where models are trained per category. Further details on these subsets are provided in the supp. material.

**Metrics.** In our evaluation, we adhere to the metrics established in DexGraspNet, ensuring a fair comparison with baseline methods. These metrics encompass two key aspects: quality and diversity. To assess grasp quality, three metrics are used: 1) *Success rate (%)*: A grasp is considered successful if it can endure at least one of the six gravity directions in the Isaac Gym simulator and exhibits a maximal penetration depth of less than 0.5 cm. 2) *Mean  $Q_1$* :  $Q_1$  [14] is defined as the radius of the inscribed sphere of ConvexHull ( $\cup_i w_i$ ), representing the norm of the smallest wrench that can destabilize the grasp. The contact threshold is set to 1cm. 3) *Maximal penetration depth (cm)*: The maximal penetration depth is calculated as the penetration depth from the object point cloud to the hand meshes. *Diversity* is evaluated through joint angle entropy. The joint motion range is discretized into 100 bins, and all generated samples contribute to estimating a probability distribution. The entropy is then computed as the entropy of these distributions. The reported value represents the mean and standard deviation across all joints.

**Baseline Methods.** To the best of our knowledge, only two competitive methods have been fully evaluated on DexGraspNet: DDG [33] and GraspTTA [21]. DDG [33] introduces a differentiable  $Q_1$  metric and supervises a regression-based network to predict grasps end-to-end. The network takes a set of five depth images as input and regresses the pose and joint angles for one grasp. GraspTTA [21] follows a two-stage training strategy. It generates a coarse grasp conditioned on the point cloud of a given object through a CVAE network initially, followed by a contact net to predict a contact map. The contact anchors, along with the penetration energy, are introduced to a test-time adaption stage where the grasp undergoes final refinement.

## 6.2. Results of Dexterous Grasping

**Quantitative Results.** The quantitative results, as depicted in Tab. 1, underscore the superior performance of UGG compared to baseline methods. The performance metrics for the baseline methods are referenced from the DexGraspNet [71] benchmark. UGG achieves the highest success rate (72.7%),  $Q_1$  (0.063), and the lowest penetration (0.14) among all methods. In terms of diversity, UGG outperforms

	Quality			Diversity	
	success $\uparrow$	$Q_1$ $\uparrow$	pen $\downarrow$	H mean $\uparrow$	H std $\downarrow$
DDG [33]	67.5	0.058	0.17	5.68	1.99
GraspTTA [21]	24.5	0.027	0.68	6.11	0.56
UGG (w/o disc)	64.1	0.036	0.17	<b>8.31</b>	0.28
UGG (ours)	<b>72.7</b>	<b>0.063</b>	<b>0.14</b>	7.17	<b>0.07</b>

Table 1. Quantitative results of grasp generation of UGG and benchmark methods on the DexGraspNet.

DDG and GraspTTA significantly, demonstrating superiority in both mean entropy (7.17) and standard deviation (0.07). This highlights the efficacy of the proposed unified diffusion model. In particular, even without the proposed physics discriminator, our method achieves a success rate of 64.1%, only marginally trailing the DDG method. Our approach, drawing insights from both generative and regression-based models, establishes itself as a state-of-the-art performer in terms of both quality and diversity. For seen categories, our method achieves an average success rate of 73.8%, while for novel categories, our model achieves a success rate of 68.1%. These results underscore the strong generalizability of UGG to novel categories.

**Qualitative Results.** Fig. 4 illustrates the grasps generated by UGG. The top two rows display results for objects within seen categories (though not part of the training set), while the bottom row showcases results for objects falling under novel categories not encountered during training. Each object is accompanied by three distinct generated grasps, highlighting the considerable diversity of the generated grasps. We highlight the depiction of mugs in the middle, emphasizing the model’s capacity to encompass even the handle in its generated grasps. Another noteworthy instance is the headphone in the top right corner, where the generative model exhibits proficiency in devising grasping approaches involving both earpads and the headband.

Additionally, Fig. 5 depicts the generated contact anchors. These anchors signify crucial positions for the grasping task, and our hand model adeptly conforms to these positions. The generated contact anchors demonstrate high diversity, preventing the generated grasps from being confined to fixed poses. Even for unseen objects, such as the bunny car on the right, the contact anchors approach the object and identify valuable grasping points. Some contact anchors may appear close to each other, a natural occurrence based on the relatively strict threshold used in computing the training data. This threshold is set to align with the precise nature of the grasping task.

## 6.3. Other Generative Results

In addition to the well-defined task of dexterous grasping by hand generation, the proposed framework can also generate objects based on a given hand, or a pair of an object and a hand from scratch. Both exhibit a successful grasping. In this part, we show the qualitative results of these

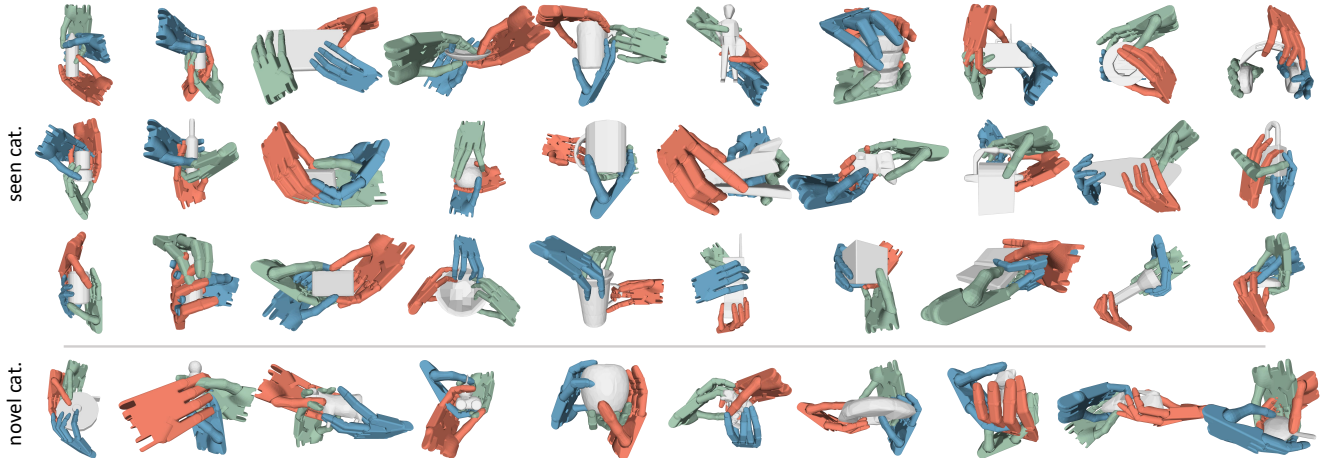


Figure 4. Visualization of the generated diverse grasps of UGG on the DexGraspNet objects (mesh used only for visualization). Top: grasps of objects from seen categories; Bottom: grasps for objects of novel categories.

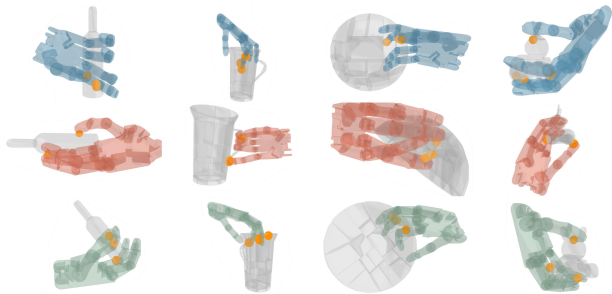


Figure 5. Visualization of *Contact Anchor*. The yellow points are the generated contact anchors. Zoom in for a better view.

generations. The mesh is constructed based on the generated point cloud using the off-the-shelf method *Shape As Points* (SAP) [48].

**Object Generation.** In Fig. 6, we present the results of object generation based on the hand poses provided using three models trained on *the entire dataset*, the *20 objects subset*, and the *10 bottles subset*, respectively. The tests maintain consistent hand joint parameters for each model (in each column), with variations in rotation and translation.

Overall, the models exhibit the capability to generate valid objects corresponding to the given hand poses. We observe that objects generated from the entire dataset predominantly take on the form of small cubes that fit within the hand without extending significantly beyond. Several explanations emerge: 1) the entire dataset comprises a substantial number of objects with an abstract cube-like shape. 2) Learning to grasp on the entire dataset enables the model to grasp the abstract concept of a graspable shape for object generation. 3) The “graspability” of an object is primarily determined by the portion within the hand. These generation results provide insight into how the model perceives the object during hand pose generation, offering a valuable perspective for designing more efficient 3D representations

in grasping tasks.

When presented with a smaller subset of objects, our model demonstrates the ability to generate a diverse range of objects across different categories, as evidenced in the middle and bottom rows of Fig. 6. This aligns with the common practice in point cloud generation methods to operate on a per-category basis. Objects such as bowl, plate, and mug in the second row demonstrate a design adapted to the hand pose. The leftmost bottle in the third row, with a slight bump on the right for holding, further showcases the potential of our models in human-centric object design.

**Joint Generation.** Fig. 7 showcases the results of joint generation of objects and hands. We exclude the model trained on the entire dataset, as explained earlier, due to its consistent generation of cube-like objects. The visualization highlights the generation of a diverse array of objects and hand poses concurrently. This capacity contributes valuable additional data pairs to the grasping task, even when provided with a minimal initial dataset.

#### 6.4. Ablation Study

**Physics Discriminator.** We conduct an ablation study on the physics discriminator to assess its performance and how the hyper-parameter influences the quantitative results. We consider two settings: 1) Setting different thresholds for predicted probabilities and 2) Selecting a different number of poses by ranking the predicted probabilities. A good discriminator is expected to show an increasing success rate with an increase in the threshold and a decreasing success rate with a larger number of selected poses. We generated a total of 1000 poses for this study.

Fig. 8 presents the results in these settings. The performance of our physics discriminator aligns with the anticipated behavior of a competent discriminator. Noteworthy observations include that more than half of the generated

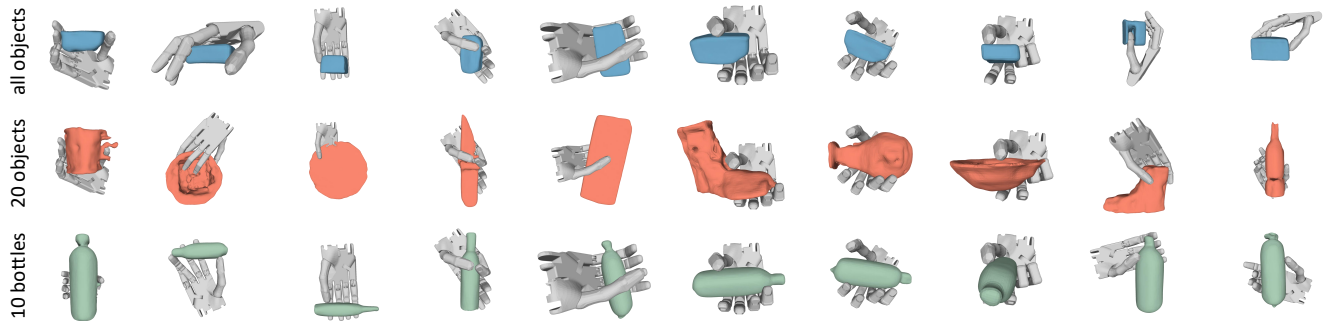


Figure 6. Visualization of object generation by UGG across three subsets, utilizing grey hand poses subjected to different transformations. The hand poses within each column are the same. The top row presents the results of the model trained on the entire dataset, while the middle and bottom rows exhibit the results of the models trained on subsets comprising 20 objects and 10 bottles, respectively.

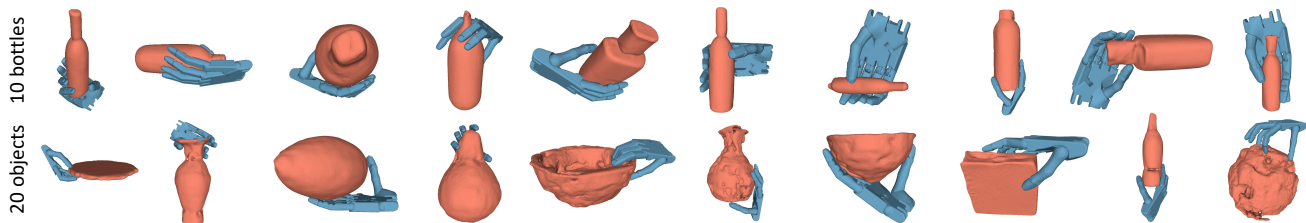


Figure 7. Joint generation visualization of UGG, illustrating simultaneous generation of hand and objects. Results are presented for models trained on two subsets.

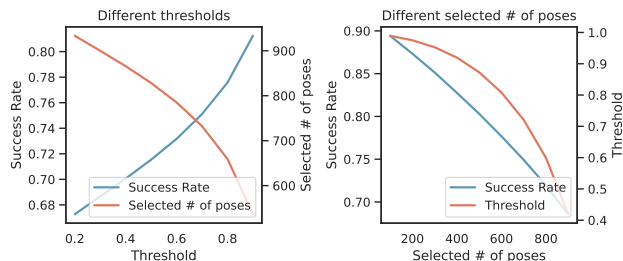


Figure 8. Success rate after the discriminator. Left: over the changes of threshold; Right: over the number of selected poses.

hand encoder	contact anchor	Quality			Diversity	
		success $\uparrow$	$Q_1$ $\uparrow$	pen $\downarrow$	H mean $\uparrow$	H std $\downarrow$
$\checkmark$		54.3	0.061	0.15	7.92	0.24
$\checkmark$		53.5	<b>0.072</b>	0.18	7.98	0.21
$\checkmark$	$\checkmark$	<b>59.9</b>	0.037	<b>0.16</b>	<b>7.99</b>	<b>0.19</b>

Table 2. The effectiveness of different generative model components. Results are shown on a 20-object subset.

poses have a confidence score exceeding 0.9, with more than 81% of them being successful. This is attributed to the robust nature of our generation module. Furthermore, for a specific grasping task, simultaneously generating multiple poses and selecting the highest confidence of the physics discriminator can significantly improve the success rate. We believe there is substantial potential in developing physics discriminators to assist in real-world pose generation tasks.

**Ablation on Hand Encoder and Contact Anchor.** To assess the effectiveness of each component in our UGG model, we conduct an ablation study on the generative model. The baseline model comprises a unified generation model without incorporating hand joint encoding or using the contact anchor. Another baseline model includes the hand joint encoder but excludes the use of the contact anchor. Given the complexity of the extensive dataset, we train and test three models on a smaller subset involving 20 objects, with details provided in the appendix. Each model undergoes testing without the physics discriminator to ensure a fair comparison of its generative performance.

Tab. 2 presents results, revealing that the model incorporating both components surpasses the two baseline methods in both success rate and diversity. This superiority is attributed to the effectiveness of the proposed contact anchors, which provide valuable guidance for grasp generation during the generation and optimization phases. The model with the hand encoder does not demonstrate significant difference in success rate but enhances diversity compared to the model without the hand encoder. The encoding of hand joint parameters is akin to a data augmentation method, introducing increased diversity. It should be noted that the baseline method without the hand encoder and contact anchor can be considered as a variant of the method proposed in SceneDiffuser [20] (reproducing SceneDiffuser in this dataset is not feasible). This ablation study high-

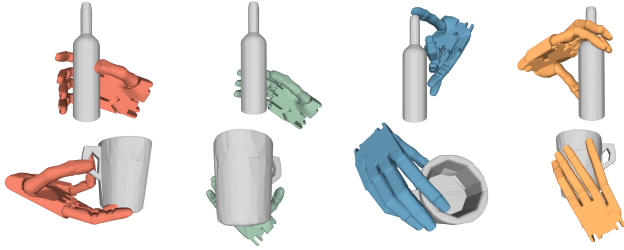


Figure 9. Failure case analysis of UGG. We show four types of failure cases in the generation process. **Red**: Succeeded in the simulator but the penetration is considered too large. **Green**: Hand detached from the object. **Blue**: More of a touch instead of a grasp, yet could fool the discriminator. **Yellow**: A valid grasp from simulation but considered as a failure by the physics discriminator.

lights the substantial contributions of our proposed encoding schemes and contact modeling to the success of UGG.

**Limitation and Failure Case Analysis.** Fig. 9 presents a comprehensive exploration of four prominent failure types identified in our generation results. A noteworthy challenge arises when certain generated poses exhibit substantial penetration between the hand and the object (red), contrasting cases where the hand and object become completely detached (green). An intriguing observation within the generation results is the existence of grasps that lean more towards a touch rather than a comprehensive grasp (blue), such results can sometimes even fool our physics discriminator. Additionally, we visualize instances where the discriminator erroneously categorizes generated grasps capable of holding the object as negative samples (yellow). In general, most of the presented cases only require subtle adjustments to be valid. Although our methodology currently stands as the state-of-the-art in dexterous grasping, we acknowledge the need for future endeavors to refine the physics discriminator and strike a more optimal balance between penetration, simulated success, and grasp diversity.

## 7. Conclusions

This work tackles the task of dexterous grasping. By introducing a novel representation of contact information, *Contact Anchor*, for the first time, it models objects, hands, and contacts in a unified diffusion process. A physics discriminator is carefully designed to utilize the diversity of a generative model, and further push the success rate of grasping. The combining of all these novelties results in an effective framework that outperforms all state-of-the-art results on both success rate and diversity. In addition, grasping generation from hand to object, or even both from scratch, becomes possible, with the help of the proposed unified design.

## References

- [1] Chen Bao, Helin Xu, Yuzhe Qin, and Xiaolong Wang. Dextart: Benchmarking generalizable dexterous manipulation with articulated objects. In *Proceedings of the IEEE/CVF Conference on Computer Vision and Pattern Recognition*, pages 21190–21200, 2023. 1
- [2] Fan Bao, Chongxuan Li, Yue Cao, and Jun Zhu. All are worth words: a vit backbone for score-based diffusion models. In *NeurIPS 2022 Workshop on Score-Based Methods*, 2022. 3, 4
- [3] Fan Bao, Shen Nie, Kaiwen Xue, Chongxuan Li, Shiliang Pu, Yaole Wang, Gang Yue, Yue Cao, Hang Su, and Jun Zhu. One transformer fits all distributions in multi-modal diffusion at scale. In *International Conference on Machine Learning*, 2023. 2, 3, 4
- [4] Lars Berscheid, Pascal Meißner, and Torsten Kröger. Self-supervised learning for precise pick-and-place without object model. *IEEE Robotics and Automation Letters*, 5(3):4828–4835, 2020. 1
- [5] Samarth Brahmabhatt, Ankur Handa, James Hays, and Dieter Fox. Contactgrasp: Functional multi-finger grasp synthesis from contact. In *2019 IEEE/RSJ International Conference on Intelligent Robots and Systems (IROS)*, pages 2386–2393. IEEE, 2019. 2
- [6] Shang Chai, Liansheng Zhuang, and Fengying Yan. Layoutdm: Transformer-based diffusion model for layout generation. In *Proceedings of the IEEE/CVF Conference on Computer Vision and Pattern Recognition (CVPR)*, pages 18349–18358, June 2023. 2
- [7] Angel X. Chang, Thomas Funkhouser, Leonidas Guibas, Pat Hanrahan, Qixing Huang, Zimo Li, Silvio Savarese, Manolis Savva, Shuran Song, Hao Su, Jianxiong Xiao, Li Yi, and Fisher Yu. ShapeNet: An Information-Rich 3D Model Repository. Technical Report arXiv:1512.03012 [cs.GR], Stanford University — Princeton University — Toyota Technological Institute at Chicago, 2015. 14
- [8] Yen-Chi Cheng, Hsin-Ying Lee, Sergey Tulyakov, Alexander G. Schwing, and Liang-Yan Gui. Sdfusion: Multimodal 3d shape completion, reconstruction, and generation. In *Proceedings of the IEEE/CVF Conference on Computer Vision and Pattern Recognition (CVPR)*, pages 4456–4465, June 2023. 2
- [9] Gene Chou, Yuval Bahat, and Felix Heide. Diffusion-sdf: Conditional generative modeling of signed distance functions. In *The IEEE International Conference on Computer Vision (ICCV)*, 2023. 2
- [10] Matei Ciocarlie, Corey Goldfeder, and Peter Allen. Dexterous grasping via eigengrasps: A low-dimensional approach to a high-complexity problem. In *Robotics: Science and systems manipulation workshop-sensing and adapting to the real world*, 2007. 2
- [11] Hongkai Dai, Anirudha Majumdar, and Russ Tedrake. Synthesis and optimization of force closure grasps via sequential semidefinite programming. In *ISRR (1)*, volume 2 of *Springer Proceedings in Advanced Robotics*, pages 285–305. Springer, 2015. 1, 2

- [12] Mehmet Dogar, Andrew Spielberg, Stuart Baker, and Daniela Rus. Multi-robot grasp planning for sequential assembly operations. *Autonomous Robots*, 43:649–664, 2019. [1](#)
- [13] Pan Fan, Bin Yan, Meirong Wang, Xiaoyan Lei, Zhijie Liu, and Fuzeng Yang. Three-finger grasp planning and experimental analysis of picking patterns for robotic apple harvesting. *Computers and Electronics in Agriculture*, 188:106353, 2021. [1](#)
- [14] C. Ferrari and J. Canny. Planning optimal grasps. In *Proceedings 1992 IEEE International Conference on Robotics and Automation*, pages 2290–2295 vol.3, 1992. [6](#)
- [15] Patrick Grady, Chengcheng Tang, Christopher D. Twigg, Minh Vo, Samarth Brahmabhatt, and Charles C. Kemp. ContactOpt: Optimizing contact to improve grasps. In *Conference on Computer Vision and Pattern Recognition (CVPR)*, 2021. [2](#), [3](#), [4](#)
- [16] Anchit Gupta, Wenhan Xiong, Yixin Nie, Ian Jones, and Barlas Oğuz. 3dgen: Triplane latent diffusion for textured mesh generation. *arXiv preprint arXiv:2303.05371*, 2023. [2](#)
- [17] Jonathan Ho, Ajay Jain, and Pieter Abbeel. Denoising diffusion probabilistic models. *Advances in neural information processing systems*, 33:6840–6851, 2020. [2](#)
- [18] Jonathan Ho, Ajay Jain, and Pieter Abbeel. Denoising diffusion probabilistic models. *arXiv preprint arxiv:2006.11239*, 2020. [13](#), [14](#)
- [19] Jiaheng Hu, David Watkins, and Peter Allen. Teleoperated robot grasping in virtual reality spaces, 2023. [1](#)
- [20] Siyuan Huang, Zan Wang, Puhao Li, Baoxiong Jia, Tengyu Liu, Yixin Zhu, Wei Liang, and Song-Chun Zhu. Diffusion-based generation, optimization, and planning in 3d scenes. In *Proceedings of the IEEE/CVF Conference on Computer Vision and Pattern Recognition (CVPR)*, 2023. [2](#), [8](#)
- [21] Hanwen Jiang, Shaowei Liu, Jiashun Wang, and Xiaolong Wang. Hand-object contact consistency reasoning for human grasps generation. In *Proceedings of the International Conference on Computer Vision*, 2021. [1](#), [2](#), [3](#), [4](#), [5](#), [6](#)
- [22] Korrawe Karunratanakul, Jinlong Yang, Yan Zhang, Michael J. Black, Krikamol Muandet, and Siyu Tang. Grasping field: Learning implicit representations for human grasps. *2020 International Conference on 3D Vision (3DV)*, pages 333–344, 2020. [2](#), [3](#), [4](#)
- [23] Bahjat Kawar, Shiran Zada, Oran Lang, Omer Tov, Huiwen Chang, Tali Dekel, Inbar Mosseri, and Michal Irani. Imagic: Text-based real image editing with diffusion models. In *Proceedings of the IEEE/CVF Conference on Computer Vision and Pattern Recognition (CVPR)*, pages 6007–6017, June 2023. [2](#)
- [24] Uikyum Kim, Dawoon Jung, Heeyoen Jeong, Jongwoo Park, Hyun-Mok Jung, Joono Cheong, Hyouk Ryeol Choi, Hyunmin Do, and Chanhun Park. Integrated linkage-driven dexterous anthropomorphic robotic hand. *Nature communications*, 12(1):7177, 2021. [1](#)
- [25] Diederik P. Kingma and Jimmy Ba. Adam: A method for stochastic optimization. In Yoshua Bengio and Yann LeCun, editors, *3rd International Conference on Learning Representations, ICLR 2015, San Diego, CA, USA, May 7-9, 2015, Conference Track Proceedings*, 2015. [5](#)
- [26] Diederik P Kingma and Max Welling. Auto-encoding variational bayes. *arXiv preprint arXiv:1312.6114*, 2013. [2](#), [3](#)
- [27] Robert Krug, Dimitar Dimitrov, Krzysztof Charusta, and Boyko Iliev. On the efficient computation of independent contact regions for force closure grasps. In *2010 IEEE/RSJ International Conference on Intelligent Robots and Systems*, pages 586–591, 2010. [2](#)
- [28] Kelin Li, Nicholas Baron, Xian Zhang, and Nicolas Rojas. Efficientgrasp: A unified data-efficient learning to grasp method for multi-fingered robot hands. *IEEE Robotics and Automation Letters*, 7(4):8619–8626, 2022. [2](#)
- [29] Puhao Li, Tengyu Liu, Yuyang Li, Yiran Geng, Yixin Zhu, Yaodong Yang, and Siyuan Huang. Gendexgrasp: Generalizable dexterous grasping. In *2023 IEEE International Conference on Robotics and Automation (ICRA)*, pages 8068–8074, 2023. [2](#)
- [30] Chen-Hsuan Lin, Jun Gao, Luming Tang, Towaki Takikawa, Xiaohui Zeng, Xun Huang, Karsten Kreis, Sanja Fidler, Ming-Yu Liu, and Tsung-Yi Lin. Magic3d: High-resolution text-to-3d content creation. In *Proceedings of the IEEE/CVF Conference on Computer Vision and Pattern Recognition (CVPR)*, pages 300–309, June 2023. [2](#)
- [31] Huan Liu, Mario Selvaggio, Pasquale Ferrentino, Rocco Moccia, Salvatore Pirozzi, Umberto Bracale, and Fanny Ficuciello. The musha hand ii: a multifunctional hand for robot-assisted laparoscopic surgery. *IEEE/ASME Transactions on Mechatronics*, 26(1):393–404, 2021. [1](#)
- [32] Min Liu, Zherong Pan, Kai Xu, Kanishka Ganguly, and Dinesh Manocha. Generating grasp poses for a high-dof gripper using neural networks. In *2019 IEEE/RSJ International Conference on Intelligent Robots and Systems (IROS)*, pages 1518–1525. IEEE, 2019. [2](#)
- [33] Min Liu, Zherong Pan, Kai Xu, Kanishka Ganguly, and Dinesh Manocha. Deep differentiable grasp planner for high-dof grippers. *ArXiv*, abs/2002.01530, 2020. [1](#), [2](#), [6](#), [15](#)
- [34] Shaowei Liu, Yang Zhou, Jimei Yang, Saurabh Gupta, and Shenlong Wang. Contactgen: Generative contact modeling for grasp generation. In *Proceedings of the IEEE/CVF International Conference on Computer Vision*, 2023. [2](#), [3](#), [4](#)
- [35] Tengyu Liu, Zeyu Liu, Ziyuan Jiao, Yixin Zhu, and Song-Chun Zhu. Synthesizing diverse and physically stable grasps with arbitrary hand structures using differentiable force closure estimator. *IEEE Robotics and Automation Letters*, 7(1):470–477, 2021. [2](#)
- [36] Zhen Liu, Yao Feng, Michael J. Black, Derek Nowrouzezahrai, Liam Paull, and Weiyang Liu. Meshdiffusion: Score-based generative 3d mesh modeling. In *International Conference on Learning Representations*, 2023. [2](#)
- [37] Zhijian Liu, Haotian Tang, Yujun Lin, and Song Han. Pointvoxel cnn for efficient 3d deep learning. In *Advances in Neural Information Processing Systems*, 2019. [4](#)
- [38] Jens Lundell, Enric Corona, Tran Nguyen Le, Francesco Verdoja, Philippe Weinzaepfel, Grégory Rogez, Francesc Moreno-Noguer, and Ville Kyrki. Multi-fingan: Generative coarse-to-fine sampling of multi-finger grasps. In *2021 IEEE International Conference on Robotics and Automation (ICRA)*, pages 4495–4501. IEEE, 2021. [2](#)

- [39] Jens Lundell, Francesco Verdoja, and Ville Kyrki. Ddgc: Generative deep dexterous grasping in clutter. *IEEE Robotics and Automation Letters*, 6(4):6899–6906, 2021. 2
- [40] Shitong Luo and Wei Hu. Diffusion probabilistic models for 3d point cloud generation. In *Proceedings of the IEEE/CVF Conference on Computer Vision and Pattern Recognition*, pages 2837–2845, 2021. 2
- [41] Zhaoyang Lyu, Jinyi Wang, Yuwei An, Ya Zhang, Dahua Lin, and Bo Dai. Controllable mesh generation through sparse latent point diffusion models. In *Proceedings of the IEEE/CVF Conference on Computer Vision and Pattern Recognition*, pages 271–280, 2023. 2
- [42] Zhaoyang Lyu, Jinyi Wang, Yuwei An, Ya Zhang, Dahua Lin, and Bo Dai. Controllable mesh generation through sparse latent point diffusion models, 2023. 6
- [43] Viktor Makoviychuk, Lukasz Wawrzyniak, Yunrong Guo, Michelle Lu, Kier Storey, Miles Macklin, David Hoeller, Nikita Rudin, Arthur Allshire, Ankur Handa, et al. Isaac gym: High performance gpu-based physics simulation for robot learning. *arXiv preprint arXiv:2108.10470*, 2021. 3, 5
- [44] Priyanka Mandikal and Kristen Grauman. Learning dexterous grasping with object-centric visual affordances. In *2021 IEEE international conference on robotics and automation (ICRA)*, pages 6169–6176. IEEE, 2021. 2
- [45] A.T. Miller and P.K. Allen. Graspit! a versatile simulator for robotic grasping. *IEEE Robotics and Automation Magazine*, 11(4):110–122, 2004. 2
- [46] Norman Müller, Yawar Siddiqui, Lorenzo Porzi, Samuel Rota Buló, Peter Kotschieder, and Matthias Nießner. Diffrf: Rendering-guided 3d radiance field diffusion. In *Proceedings of the IEEE/CVF Conference on Computer Vision and Pattern Recognition*, pages 4328–4338, 2023. 2
- [47] Rhys Newbury, Morris Gu, Lachlan Chumbley, Arsalan Mousavian, Clemens Eppner, Jürgen Leitner, Jeannette Bohg, Antonio Morales, Tamim Asfour, Danica Kragic, et al. Deep learning approaches to grasp synthesis: A review. *IEEE Transactions on Robotics*, 2023. 2
- [48] Songyou Peng, Chiyu “Max” Jiang, Yiyi Liao, Michael Niemeyer, Marc Pollefeys, and Andreas Geiger. Shape as points: A differentiable poisson solver. In *Advances in Neural Information Processing Systems (NeurIPS)*, 2021. 7, 14
- [49] Domenico Prattichizzo, Monica Malvezzi, Marco Gabiccini, and Antonio Bicchi. On the manipulability ellipsoids of underactuated robotic hands with compliance. *Robotics and Autonomous Systems*, 60(3):337–346, 2012. 2
- [50] Charles Ruizhongtai Qi, Li Yi, Hao Su, and Leonidas J Guibas. Pointnet++: Deep hierarchical feature learning on point sets in a metric space. *Advances in neural information processing systems*, 30, 2017. 5, 15
- [51] Alberto Rodriguez, Matthew T Mason, and Steve Ferry. From caging to grasping. *The International Journal of Robotics Research*, 31(7):886–900, 2012. 2
- [52] Robin Rombach, Andreas Blattmann, Dominik Lorenz, Patrick Esser, and Björn Ommer. High-resolution image synthesis with latent diffusion models. In *Proceedings of the IEEE/CVF conference on computer vision and pattern recognition*, pages 10684–10695, 2022. 2
- [53] Javier Romero, Dimitrios Tzionas, and Michael J. Black. Embodied hands: Modeling and capturing hands and bodies together. *ACM Trans. Graph.*, 36(6), nov 2017. 2
- [54] Carlos Rosales, Raúl Suárez, Marco Gabiccini, and Antonio Bicchi. On the synthesis of feasible and prehensile robotic grasps. In *2012 IEEE international conference on robotics and automation*, pages 550–556. IEEE, 2012. 2
- [55] Nataniel Ruiz, Yuanzhen Li, Varun Jampani, Yael Pritch, Michael Rubinstein, and Kfir Aberman. Dreambooth: Fine tuning text-to-image diffusion models for subject-driven generation. In *Proceedings of the IEEE/CVF Conference on Computer Vision and Pattern Recognition (CVPR)*, pages 22500–22510, June 2023. 2
- [56] Chitwan Saharia, William Chan, Saurabh Saxena, Lala Li, Jay Whang, Emily L Denton, Kamyar Ghasemipour, Raphael Gontijo Lopes, Burcu Karagol Ayan, Tim Salimans, et al. Photorealistic text-to-image diffusion models with deep language understanding. *Advances in Neural Information Processing Systems*, 35:36479–36494, 2022. 2
- [57] Shadowhand. <https://www.shadowrobot.com/dexterous-hand-series/>, 2005. 2, 4, 5
- [58] Lin Shao, Fabio Ferreira, Mikael Jorda, Varun Nambiar, Jianlan Luo, Eugen Solowjow, Juan Aparicio Ojea, Oussama Khatib, and Jeannette Bohg. Unigrasp: Learning a unified model to grasp with multifingered robotic hands. *IEEE Robotics and Automation Letters*, 5(2):2286–2293, 2020. 2
- [59] J. Ryan Shue, Eric Ryan Chan, Ryan Po, Zachary Ankner, Jiajun Wu, and Gordon Wetzstein. 3d neural field generation using triplane diffusion. In *Proceedings of the IEEE/CVF Conference on Computer Vision and Pattern Recognition (CVPR)*, pages 20875–20886, June 2023. 2
- [60] Jaskirat Singh, Stephen Gould, and Liang Zheng. High-fidelity guided image synthesis with latent diffusion models. In *2023 IEEE/CVF Conference on Computer Vision and Pattern Recognition (CVPR)*, pages 5997–6006. IEEE, 2023. 2
- [61] Jascha Sohl-Dickstein, Eric Weiss, Niru Maheswaranathan, and Surya Ganguli. Deep unsupervised learning using nonequilibrium thermodynamics. In Francis Bach and David Blei, editors, *Proceedings of the 32nd International Conference on Machine Learning*, volume 37 of *Proceedings of Machine Learning Research*, pages 2256–2265, Lille, France, 07–09 Jul 2015. PMLR. 13
- [62] Jiaming Song, Chenlin Meng, and Stefano Ermon. Denoising diffusion implicit models. *arXiv preprint arXiv:2010.02502*, 2020. 2
- [63] Jiaming Song, Chenlin Meng, and Stefano Ermon. Denoising diffusion implicit models. In *International Conference on Learning Representations*, 2021. 14
- [64] Yang Song, Jascha Sohl-Dickstein, Diederik P Kingma, Abhishek Kumar, Stefano Ermon, and Ben Poole. Score-based generative modeling through stochastic differential equations. *arXiv preprint arXiv:2011.13456*, 2020. 2
- [65] Dylan Turpin, Liquan Wang, Eric Heiden, Yun-Chun Chen, Miles Macklin, Stavros Tsogkas, Sven Dickinson, and Animesh Garg. Grasp’d: Differentiable contact-rich grasp synthesis for multi-fingered hands. In *European Conference on Computer Vision*, pages 201–221. Springer, 2022. 1, 2

- [66] Dylan Turpin, Tao Zhong, Shutong Zhang, Guanglei Zhu, Eric Heiden, Miles Macklin, Stavros Tsogkas, Sven Dickinson, and Animesh Garg. Fast-grasp’d: Dexterous multi-finger grasp generation through differentiable simulation. In *ICRA*, 2023. 2
- [67] Julen Urain, Niklas Funk, Georgia Chalvatzaki, and Jan Peters. Se (3)-diffusionfields: Learning cost functions for joint grasp and motion optimization through diffusion. *arXiv preprint arXiv:2209.03855*, 2022. 2
- [68] Jacob Varley, Jonathan Weisz, Jared Weiss, and Peter Allen. Generating multi-fingered robotic grasps via deep learning. In *2015 IEEE/RSJ International Conference on Intelligent Robots and Systems (IROS)*, pages 4415–4420, 2015. 2
- [69] Ashish Vaswani, Noam Shazeer, Niki Parmar, Jakob Uszkoreit, Llion Jones, Aidan N Gomez, Łukasz Kaiser, and Illia Polosukhin. Attention is all you need. *Advances in neural information processing systems*, 30, 2017. 2
- [70] Weikang Wan, Haoran Geng, Yun Liu, Zikang Shan, Yaodong Yang, Li Yi, and He Wang. Unidexgrasp++: Improving dexterous grasping policy learning via geometry-aware curriculum and iterative generalist-specialist learning. *arXiv preprint arXiv:2304.00464*, 2023. 1
- [71] Ruicheng Wang, Jialiang Zhang, Jiayi Chen, Yinzheng Xu, Puhao Li, Tengyu Liu, and He Wang. Dexgraspnet: A large-scale robotic dexterous grasp dataset for general objects based on simulation. In *2023 IEEE International Conference on Robotics and Automation (ICRA)*, pages 11359–11366. IEEE, 2023. 1, 2, 3, 5, 6, 15, 16
- [72] Qihong Anna Wei, Sijie Ding, Jeong Joon Park, Rahul Sajjani, Adrien Poulenard, Srinath Sridhar, and Leonidas Guibas. Lego-net: Learning regular rearrangements of objects in rooms. *arXiv preprint arXiv:2301.09629*, 2023. 2
- [73] Wei Wei, Daheng Li, Peng Wang, Yiming Li, Wanyi Li, Yongkang Luo, and Jun Zhong. Dvvg: Deep variational grasp generation for dextrous manipulation. *IEEE Robotics and Automation Letters*, 7(2):1659–1666, 2022. 2
- [74] Jiale Xu, Xintao Wang, Weihao Cheng, Yan-Pei Cao, Ying Shan, Xiaohu Qie, and Shenghua Gao. Dream3d: Zero-shot text-to-3d synthesis using 3d shape prior and text-to-image diffusion models. In *Proceedings of the IEEE/CVF Conference on Computer Vision and Pattern Recognition (CVPR)*, pages 20908–20918, June 2023. 2
- [75] Minkai Xu, Alexander Powers, Ron Dror, Stefano Ermon, and Jure Leskovec. Geometric latent diffusion models for 3d molecule generation. In *International Conference on Machine Learning*. PMLR, 2023. 2
- [76] Xingqian Xu, Zhangyang Wang, Gong Zhang, Kai Wang, and Humphrey Shi. Versatile diffusion: Text, images and variations all in one diffusion model. In *Proceedings of the IEEE/CVF International Conference on Computer Vision*, pages 7754–7765, 2023. 2
- [77] Yinzheng Xu, Weikang Wan, Jialiang Zhang, Haoran Liu, Zikang Shan, Hao Shen, Ruicheng Wang, Haoran Geng, Yijia Weng, Jiayi Chen, et al. Unidexgrasp: Universal robotic dexterous grasping via learning diverse proposal generation and goal-conditioned policy. In *Proceedings of the IEEE/CVF Conference on Computer Vision and Pattern Recognition*, pages 4737–4746, 2023. 1
- [78] Xiaohui Zeng, Arash Vahdat, Francis Williams, Zan Gojcic, Or Litany, Sanja Fidler, and Karsten Kreis. Lion: Latent point diffusion models for 3d shape generation. In *Advances in Neural Information Processing Systems (NeurIPS)*, 2022. 2, 3, 4, 6, 14
- [79] He Zhang, Yuting Ye, Takaaki Shiratori, and Taku Komura. Manipnet: Neural manipulation synthesis with a hand-object spatial representation. *ACM Trans. Graph.*, 40(4), jul 2021. 1
- [80] Lvmin Zhang, Anyi Rao, and Maneesh Agrawala. Adding conditional control to text-to-image diffusion models, 2023. 2
- [81] Linqi Zhou, Yilun Du, and Jiajun Wu. 3d shape generation and completion through point-voxel diffusion. In *Proceedings of the IEEE/CVF International Conference on Computer Vision*, pages 5826–5835, 2021. 2
- [82] Yi Zhou, Connelly Barnes, Lu Jingwan, Yang Jimei, and Li Hao. On the continuity of rotation representations in neural networks. In *The IEEE Conference on Computer Vision and Pattern Recognition (CVPR)*, June 2019. 15
- [83] Tianqiang Zhu, Rina Wu, Jinglue Hang, Xiangbo Lin, and Yi Sun. Toward human-like grasp: Functional grasp by dexterous robotic hand via object-hand semantic representation. *IEEE Transactions on Pattern Analysis and Machine Intelligence*, 45(10):12521–12534, 2023. 1
- [84] Tianqiang Zhu, Rina Wu, Xiangbo Lin, and Yi Sun. Toward human-like grasp: Dexterous grasping via semantic representation of object-hand. In *Proceedings of the IEEE/CVF International Conference on Computer Vision*, pages 15741–15751, 2021. 2

## Appendix

### A. Generative Grasping Model

#### A.1. Introduction of Diffusion Model

Diffusion models [18, 61] perturb the data sample  $\mathbf{x}_0 \sim q(\mathbf{x}_0)$  by gradually adding noise through a fixed Markov Chain of length  $T$  formulated as:

$$q(\mathbf{x}_{1:T}|\mathbf{x}_0) = \prod_{t=1}^T q(\mathbf{x}_t|\mathbf{x}_{t-1}), \quad (6)$$

$$q(\mathbf{x}_t|\mathbf{x}_{t-1}) = \mathcal{N}(\mathbf{x}_t; \sqrt{\alpha_t}\mathbf{x}_{t-1}, \beta_t\mathbf{I}),$$

where  $q(\mathbf{x}_t|\mathbf{x}_{t-1})$  is a Gaussian transition kernel based on the variance schedule  $\beta_t$ , with  $\alpha_t = \sqrt{1 - \beta_t}$ . The generative process involves an inverted process  $p(\mathbf{x}_{t-1}|\mathbf{x}_t)$  approximated by the Gaussian model:

$$p(\mathbf{x}_0) = p(\mathbf{x}_T) \prod_{t=1}^T p(\mathbf{x}_{t-1}|\mathbf{x}_t), \quad (7)$$

$$p(\mathbf{x}_{t-1}|\mathbf{x}_t) = \mathcal{N}(\mathbf{x}_{t-1}|\boldsymbol{\mu}_t(\mathbf{x}_t), \sigma_t^2\mathbf{I}),$$

where the parametrization of  $\boldsymbol{\mu}$  satisfies

$$\boldsymbol{\mu}_t^*(\mathbf{x}_t) = \frac{1}{\sqrt{\alpha_t}} \left( \mathbf{x}_t - \frac{\beta_t}{\sqrt{1 - \bar{\alpha}_t}} \mathbb{E}[\boldsymbol{\epsilon}^x|\mathbf{x}_t] \right), \bar{\alpha}_t = \prod_{i=1}^t \alpha_i. \quad (8)$$

Here,  $\boldsymbol{\epsilon}^x$  is the Gaussian noise added to the data. This process is learned through a denoising network, also known as a noise prediction network  $\boldsymbol{\epsilon}_\xi(\mathbf{x}_t, t)$  by minimizing the variational upper bound as

$$\min_{\xi} \mathbb{E}_{\mathbf{x}_0, \boldsymbol{\epsilon}^x, t} \|\boldsymbol{\epsilon}_\xi(\mathbf{x}_t, t) - \boldsymbol{\epsilon}^x\|_2^2. \quad (9)$$

Here  $t$  is uniformly sampled from  $\{1, \dots, T\}$  and,

$$\mathbf{x}_t = \sqrt{\bar{\alpha}_t}\mathbf{x}_0 + \sqrt{1 - \bar{\alpha}_t}\boldsymbol{\epsilon}^x. \quad (10)$$

**Conditional generation** often involves modeling the conditional distribution  $q(\mathbf{x}_0|\mathbf{y}_0)$  when given a pair of data  $(\mathbf{x}_0, \mathbf{y}_0)$ , which results in a generative process denoted as  $p(\mathbf{x}_{t-1}|\mathbf{x}_t, \mathbf{y}_0)$ . The corresponding objective becomes,

$$\min_{\xi} \mathbb{E}_{\mathbf{x}_0, \mathbf{y}_0, \boldsymbol{\epsilon}^x, t} \|\boldsymbol{\epsilon}_\xi(\mathbf{x}_t, \mathbf{y}_0, t) - \boldsymbol{\epsilon}^x\|_2^2. \quad (11)$$

**Unified diffusion model** is based on the idea of conditional generation, but involves both conditional distributions  $q(\mathbf{x}_0|\mathbf{y}_0)$ ,  $q(\mathbf{y}_0|\mathbf{x}_0)$ , and the joint distribution  $q(\mathbf{x}_0, \mathbf{y}_0)$ . To achieve this, the concept of asynchronous timesteps for the data, denoted as  $t^x$  and  $t^y$ , are introduced into the diffusion models. The modeling of expectations takes on a general form expressed as  $\mathbb{E}[\boldsymbol{\epsilon}^x, \boldsymbol{\epsilon}^y|\mathbf{x}_{t^x}, \mathbf{y}_{t^y}]$ .

---

#### Algorithm 1: Training

---

```

1 repeat
2    $\mathbf{o}\mathbf{h}\mathbf{c}_0 = (\mathbf{o}_0, \mathbf{h}_0, \mathbf{c}_0) \sim q(\mathbf{o}_0, \mathbf{h}_0, \mathbf{c}_0)$ 
3    $\mathbf{t} = (t^o, t^h, t^c) \sim \text{Uniform}(\{1, \dots, T\})$ 
4    $\boldsymbol{\epsilon} = (\boldsymbol{\epsilon}^o, \boldsymbol{\epsilon}^h, \boldsymbol{\epsilon}^c) \sim \mathcal{N}(\mathbf{0}, \mathbf{I})$ 
5    $\mathbf{o}\mathbf{h}\mathbf{c}_t = \sqrt{\bar{\alpha}_t}\mathbf{o}\mathbf{h}\mathbf{c}_0 + \sqrt{1 - \bar{\alpha}_t}\boldsymbol{\epsilon}$ 
6   Take gradient step on  $\nabla_{\xi} \|\boldsymbol{\epsilon}_\xi(\mathbf{o}\mathbf{h}\mathbf{c}_t, \mathbf{t}) - \boldsymbol{\epsilon}\|_2^2$ 
7 until converged
```

---



---

#### Algorithm 2: Grasping (object) generation: sampling of hand pose $\mathbf{h}$ (object $\mathbf{o}$ ) and contact anchors $\mathbf{c}$ conditioned on object $\mathbf{o}$ (hand pose $\mathbf{h}$ )

---

```

1  $\mathbf{h}_T, \mathbf{c}_T \sim \mathcal{N}(\mathbf{0}, \mathbf{I})$ 
2 for  $t = T, \dots, 1$  do
3    $\mathbf{z}^h, \mathbf{z}^c \sim \mathcal{N}(\mathbf{0}, \mathbf{I})$  if  $t > 1$ , else  $\mathbf{z}^h, \mathbf{z}^c = \mathbf{0}$ 
4    $\mathbf{o}\mathbf{h}\mathbf{c}_t = (\mathbf{o}_0, \mathbf{h}_t, \mathbf{c}_t)$ 
5    $\mathbf{t} = (0, t, t)$ 
6    $\boldsymbol{\epsilon} = \boldsymbol{\epsilon}_\xi(\mathbf{o}\mathbf{h}\mathbf{c}, \mathbf{t})$ 
7    $\mathbf{h}_{t-1} = \frac{1}{\sqrt{\alpha_t}} \left( \mathbf{h}_t - \frac{\beta_t}{\sqrt{1 - \bar{\alpha}_t}} \boldsymbol{\epsilon}^h \right) + \sigma_t \mathbf{z}^h$ 
8    $\mathbf{c}_{t-1} = \frac{1}{\sqrt{\alpha_t}} \left( \mathbf{c}_t - \frac{\beta_t}{\sqrt{1 - \bar{\alpha}_t}} \boldsymbol{\epsilon}^c \right) + \sigma_t \mathbf{z}^c$ 
9 end
Output:  $\mathbf{h}_0, \mathbf{c}_0$ 
```

---



---

#### Algorithm 3: Joint generation: joint sampling of object $\mathbf{o}$ , hand pose $\mathbf{h}$ , and contact anchors $\mathbf{c}$

---

```

1  $\mathbf{o}\mathbf{h}\mathbf{c}_T = (\mathbf{o}_T, \mathbf{h}_T, \mathbf{c}_T) \sim \mathcal{N}(\mathbf{0}, \mathbf{I})$ 
2 for  $t = T, \dots, 1$  do
3    $\mathbf{z} = (\mathbf{z}^o, \mathbf{z}^h, \mathbf{z}^c) \sim \mathcal{N}(\mathbf{0}, \mathbf{I})$  if  $t > 1$ , else  $\mathbf{z} = \mathbf{0}$ 
4    $\mathbf{t} = (t, t, t)$ 
5    $\boldsymbol{\epsilon} = \boldsymbol{\epsilon}_\xi(\mathbf{o}\mathbf{h}\mathbf{c}_t, \mathbf{t})$ 
6    $\mathbf{o}\mathbf{h}\mathbf{c}_{t-1} = \frac{1}{\sqrt{\alpha_t}} \left( \mathbf{o}\mathbf{h}\mathbf{c}_t - \frac{\beta_t}{\sqrt{1 - \bar{\alpha}_t}} \boldsymbol{\epsilon} \right) + \sigma_t \mathbf{z}$ 
7 end
Output:  $\mathbf{o}\mathbf{h}\mathbf{c}_0 = (\mathbf{o}_0, \mathbf{h}_0, \mathbf{c}_0)$ 
```

---

Specifically, when setting  $t^y = T$ , it arrives at the approximation of the distribution  $q(\mathbf{x}_0)$  as  $\mathbb{E}[\boldsymbol{\epsilon}^x|\mathbf{x}_{t^x}, \mathbf{y}_T] \approx \mathbb{E}[\boldsymbol{\epsilon}^x|\mathbf{x}_{t^x}]$ . On the other hand, when  $t^y = 0$ ,  $\mathbb{E}[\boldsymbol{\epsilon}^x|\mathbf{x}_{t^x}, \mathbf{y}_0]$  corresponds to the conditional distribution  $q(\mathbf{x}_0|\mathbf{y}_0)$ . Setting  $t^x = t^y = t$ ,  $\mathbb{E}[\boldsymbol{\epsilon}^x, \boldsymbol{\epsilon}^y|\mathbf{x}_t, \mathbf{y}_t]$  formulates the joint distribution of  $q(\mathbf{x}_0, \mathbf{y}_0)$ . The training objective can be succinctly defined as

$$\min_{\xi} \mathbb{E}_{\mathbf{x}_0, \mathbf{y}_0, \boldsymbol{\epsilon}^x, \boldsymbol{\epsilon}^y, t^x, t^y} \|\boldsymbol{\epsilon}_\xi(\mathbf{x}_{t^x}, \mathbf{y}_{t^y}, t^x, t^y) - [\boldsymbol{\epsilon}^x, \boldsymbol{\epsilon}^y]\|_2^2 \quad (12)$$

where  $[\cdot, \cdot]$  is the concatenation.

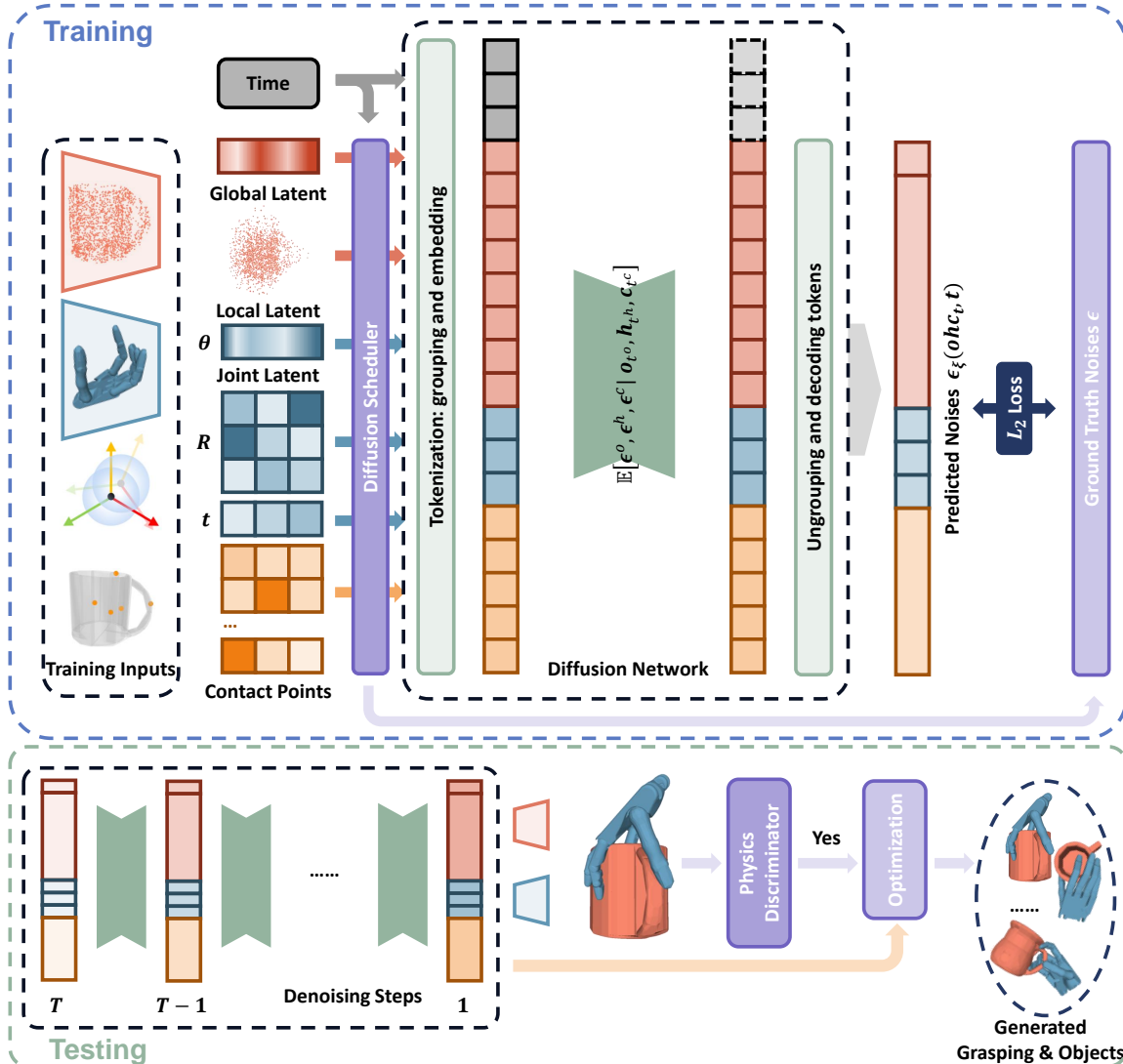


Figure 10. Details of structure of UGG and the training and testing process.

## A.2. Generation Algorithms

We provide the training algorithms in Algorithm 1. The generation process, which encompasses grasping (object) generation and joint generation using the DDPM sampler [18], is described in Algorithm 2 and Algorithm 3. It is worth noting that alternative samplers, such as DDIM [63], can be seamlessly applied to our model. However, we acknowledge that there may be performance differences when switching the sampling algorithm.

## B. Implementation

### B.1. Structure of UGG

We illustrate the network architecture in Fig. 10. This depiction aims to provide a more in-depth understanding

of our implementation. For a broader perspective on our pipeline, kindly consult Fig. 2 in our primary paper.

### B.2. Unified Shape Encoding

**Objects.** The implementation of the LION VAE [78] model strictly adheres to the official implementation open-sourced at <https://github.com/nv-tlabs/LION>. The LION VAE is trained on ShapeNet [7]. Although not fine-tuned in the DexGraspNet dataset, the model proficiently reconstructs the object point cloud on this dataset, as illustrated in Fig. 11.

Given that the LION VAE decoder yields the result in the form of a point cloud, we follow their approach of using the off-the-shelf method *Shape As Points* (SAP) [48] for object and joint generation results. The publicly avail-

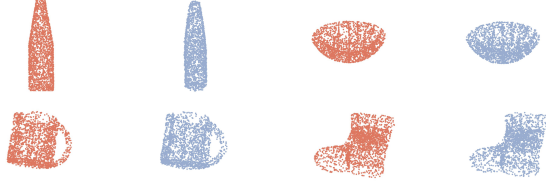


Figure 11. Visualization of the reconstruction results using LION VAE. The red point cloud represents the given point cloud sampled on the object mesh, while the blue point cloud depicts the corresponding reconstruction result.

able source code and model at [https://github.com/autonomousvision/shape\\_as\\_points](https://github.com/autonomousvision/shape_as_points) are utilized. Specifically, the *large noises* version is employed for the model trained on the *entire dataset*, while the *small noises* version is used for models trained on the *20 objects subset* and *10 bottles subset*.

**Hands.** As previously mentioned, we exclusively encode hand joint parameters  $\theta$  into the latent space using the dedicated hand VAE. The hand VAE comprises an encoder with a multilayer perceptron (MLP) of sizes [22, 32, 64] and a decoder with an MLP of sizes [64, 32, 22]. Both the encoder and decoder feature ReLU and BatchNorm between two linear layers. Each joint parameter is normalized to the range  $[-1, 1]$  before being inputted into the encoder, based on the minimum and maximum values in the data set.

For hand rotation  $R$ , we adopt the flattened 6D rotation representation [82]. Transformation  $t$  is scaled from the range  $[-0.3, 0.3]$  to  $[-1, 1]$ .

It is essential to note that our proposed method serves as a general framework for generative grasping, offering an insight for incorporating interaction information into generative grasping models. As the field progresses, and more research emerges in the 3D object generation task, there may be better or more suitable generative models for this framework. The LION and Hand VAE models presented here are one possible choice within this framework but not the exclusive option. They can be adjusted or complemented to accommodate different object modalities and hand models.

### B.3. Test-time Optimization

The test-time optimization involves penetration, self-penetration, and joint angle losses, as employed in [71],

$$\mathcal{L}_{\text{pen}} = \sum_{p \in P} \max(sd(p_i, \mathbf{S}_h), 0), \quad (13)$$

$$\mathcal{L}_{\text{spen}} = \sum_{u \in \mathbf{S}_g} \sum_{v \in \mathbf{S}_g, v \neq u} \max(\delta - d(u, v), 0), \quad (14)$$

$$\mathcal{L}_{\text{joints}} = \sum_{i=1}^k (\max(\theta_i - \theta_i^{\max}, 0) + \max(\theta_i^{\min} - \theta_i, 0)). \quad (15)$$

Parameter	UGG	description
$N$	2048	point number of input object pc
$d_g$	128	object global embedding dimension
$d_l$	1	object local embedding feature dimension
$k$	22	degree of freedom of hand model
$d_h$	64	hand joint latent dimension
$N_c$	5	number of contact anchors
$d$	512	token dimension in UViT
depth	12	depth of UViT
$T$	200	timesteps of diffusion process
$\beta_1$	0.001	the forward process variance
$\beta_T$	0.02	increasing quadratically from $\beta_1$ to $\beta_T$
$\omega_{\text{pen}}$	10	weight for penetration loss
$\omega_{\text{spen}}$	0.01	weight for self-penetration loss
$\omega_{\text{joint}}$	0.01	weight for joint angle loss
$\omega_{\text{cont}}$	10	weight for contact loss
epoch	3000	training epochs
bs	2048	total batch size
lr	0.0002	learning rate
optimizer	Adam	optimizer during training
scheduler	Cosine	learning rate scheduler
min.lr	2e-6	minimum learning rate for Cosine scheduler
$m$	40	generated grasps per object-scale pair
$n$	30	top $n$ grasp candidates from discriminator

Table 3. The detailed experiment parameters. The model, training and testing parameters are included.

Here,  $\mathbf{S}$  represents the surface of the given mesh.  $sd(\cdot, \cdot)$  represents the signed distance of a point to the given mesh surface and  $d(\cdot, \cdot)$  represents the distance between two points (or a point and a given mesh surface). The contact loss defined on our proposed contact anchors is

$$\mathcal{L}_{\text{cont}} = \sum_{i=1}^{N_c} d(c_i, \mathbf{S}_h). \quad (16)$$

The overall loss is a combination of these terms as,

$$\mathcal{L}_{\text{test}} = \omega_{\text{pen}} \mathcal{L}_{\text{pen}} + \omega_{\text{spen}} \mathcal{L}_{\text{spen}} + \omega_{\text{joint}} \mathcal{L}_{\text{joint}} + \omega_{\text{cont}} \mathcal{L}_{\text{cont}}, \quad (17)$$

Our entire pipeline only involves point cloud representation of the object, contrasting with DDG [33], whose training heavily relies on the signed distance function of the object, making it challenging to acquire related real-world data.

### B.4. Discriminator

Our discriminator adopts an architecture similar to the attention layer utilized in UViT. Specifically, the object point cloud  $\mathbf{o} \in \mathbb{R}^{N \times 3}$  is tokenized using the farthest-point sampling and k-nearest-neighbor grouping [50] into  $N_l$  tokens. The hand parameters  $\theta$ , rotation  $r$ , and transformation  $t$  are individually embedded into three tokens using a linear layer. The entire sequence is then processed through two layers of attention layer. The resultant features of the

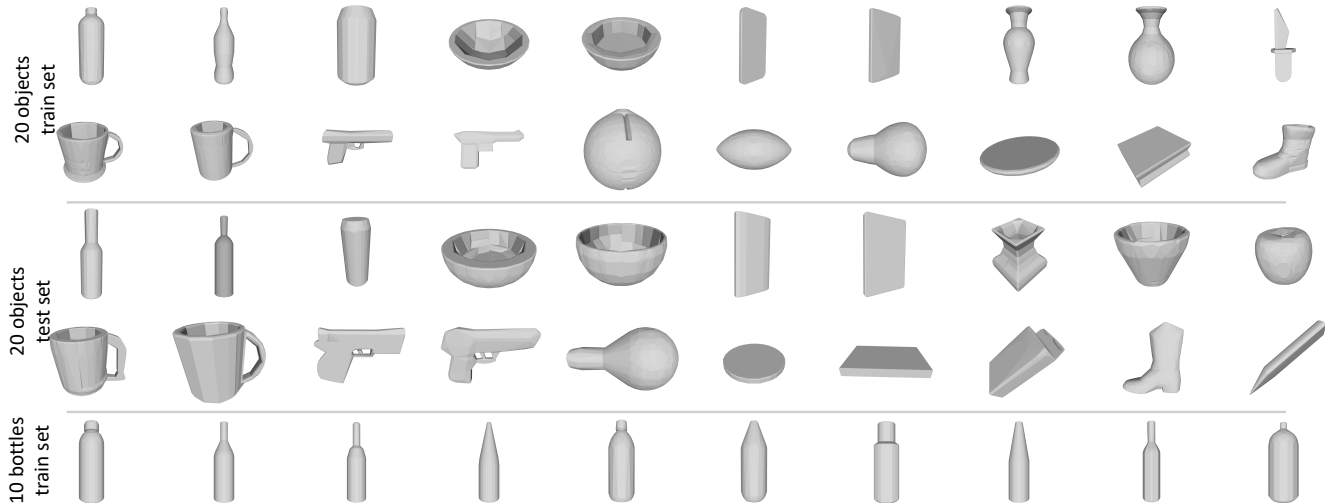


Figure 12. Visualization of all objects in the *20 objects subset* and *10 bottles subset*. The *10 bottles subset* contributes exclusively to training the object and joint generation model, involving only a training set.

object and the hand undergo separate pooling layers and are concatenated. An MLP layer is used to generate the final confidence prediction.

During the testing, we generate  $m$  grasps for each pair of objects on the object scale. All of these grasps pass through the discriminator and the top  $n$  confident grasps are selected for subsequent optimization steps.

### B.5. Model Parameters

We provide a detailed configuration of our trained model in Table 3.

## C. Experiment Details

### C.1. Dataset Setup

The DexGraspNet [71] dataset consists of 5355 objects, each associated with over 200 grasps based on 5 scales  $\{0.06, 0.08, 0.1, 0.12, 0.15\}$ . Our train/test splits adhere to those provided by the dataset. Although the original data set lacks specific information about the novel object category, we manually label the novel object category based on the provided object name code. During testing, we evenly distribute the objects of each scale.

In our ablation study, we employ two subsets of DexGraspNet: the *20 objects subset* and the *10 bottles subset*. Fig. 12 serves as a visualization reference for these two subsets. It is essential to note that the *10 bottles subset* is used exclusively for training object generation and joint generation tasks, hence providing only a training set.

### C.2. Training and Inference Time

The training of LION VAE consumes  $\approx 560$  GPU hours, whereas VAE training at the hand takes  $\approx 1.3$  GPU hours.

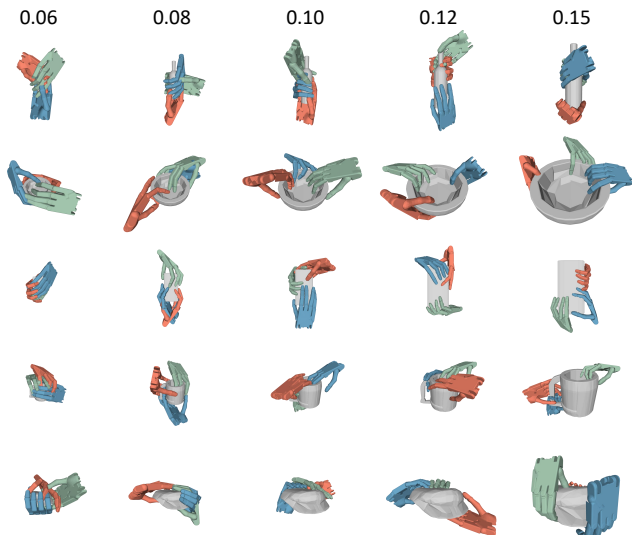


Figure 13. Visualization of grasps for a single object at various scales. Each row features the same object with five different scales in the dataset, while each column corresponds to one scale.

The training of Physics Discriminator takes  $\approx 10$  GPU hours.

For the UGG model on all DexGraspNet, the training time amounts to  $\approx 4000$  GPU hours for 3000 epochs. Training in the *20 objects subset* requires  $\approx 192$  GPU hours, and on the *10 bottles subset*, it takes  $\approx 96$  GPU hours. The inference time to generate 200 grasps (equivalent to 200 objects and 200 pairs of grasp and object generation) is roughly 66 seconds, and optimization for 100 steps requires approximately 12 seconds.

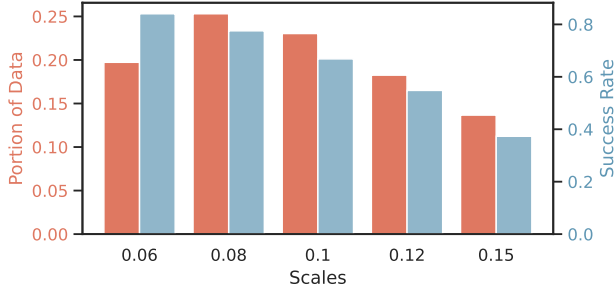


Figure 14. Data distribution and grasp generation success rate (w/o discriminator) based on object scales.

## D. Additional Results

### D.1. Grasp Generation of Different Scales

The DexGraspNet dataset comprises five scales for each object:  $\{0.06, 0.08, 0.1, 0.12, 0.15\}$ . Fig. 13 illustrates the grasp generation results for one object across these five scales. An intriguing observation emerges as the grasps on smaller-scale objects appear to be visually superior compared to those on the largest scale. To delve deeper, we analyze the dataset, examining the proportion of the data from each scale and the success rate of the grasps generated on each scale in Fig. 14. The dataset manifests an imbalance, with a higher representation of smaller-scale objects (0.06, 0.08, 0.1) and a lower representation of large-scale objects. The portion of 0.15-scale objects is merely half that of 0.08-scale objects. This skewed distribution potentially leads the model to emphasize learning from smaller-scale objects, a phenomenon reflected in the model’s performance in generating grasps for different object scales. The success rate of 0.15 scale objects is only half that of 0.06 scale objects. Furthermore, this impact extends to object generation results, as is evident in the model trained on the entire dataset, which tends to generate small, cube-like objects.